

Fig. 2: Incorporation scheme of U^{5+} into magnetite.

cally be dealt with using first principle density functional theory (DFT).

The most relevant results for the DFT calculations on pure magnetite are presented in Table 1 and 2.

The results of the structural and magnetic properties presented in Table 1 and 2 clearly show that DFT is a suitable tool to tackle pure magnetite and the study of the incorporation of U^{5+} can be carried out based on these results and with this theoretical approach.

We investigated the incorporation of U^{5+} into magnetite using the following scheme



Hence U^{5+} and one vacancy (\square) replace one Fe^{2+} and one Fe^{3+} in magnetite as shown in Figure 2 a and b. The results of the DFT calculations agree very well with the experimental results of Pidchenko *et al.* [1] (see Table 3) and allow to identify the incorporation site by comparison with the experimental results.

The best agreement between the EXAFS results and the DFT calculations are for the incorporation of U^{5+} into an octahedral Fe^{2+} site (Fe^{2+}/U^{5+} (oct)) or into an octahedral Fe^{3+} site (Fe^{3+}/U^{5+} (oct)). All other results show a less satisfying agreement with the EXAFS results and have a higher electronic energy. Hence can be excluded by these two arguments.

Furthermore, the results show that an incorporation of U^{6+} following the scheme



is less likely because the corresponding structures do not agree with the experimental findings and the much higher electronic energy.

With these calculations, we strongly support the experimental EXAFS study. The theoretical results allow an assignment of the observed structures to an incorporation scheme and thus greatly enhance the available experimental knowledge by theoretical data.

Pu(IV)-isosaccharinate complexes

D-Isosaccharinic acid (HISA) is a poly-hydroxy carboxylic acid expected in repositories for low and intermediate level waste as a degradation product of cellulosic materials in cementitious, alkaline environments [2]. Due to the large inventory of cellulose in some repository concepts and the strong complexing capacity of HISA towards hard Lewis cations, an accurate knowledge of the interaction of HISA with actinides is needed in the safety assessment of such repositories.

Solubility experiments with $Pu(IV)O_2(am,hyd)$ performed in the presence of HISA under alkaline, reducing conditions showed the predominance of two Pu(IV)-ISA species in solution. Slope analysis of the solubility data provides an unequivocal insight on the charge of these species (-1 and -2) and H^+ released in the corresponding solubility reactions, but gives no hint on the origin of the latter (either Pu^{4+} hydrolysis or deprotonation of $-OH$ groups in HISA). It is the aim of this theoretical study to determine the degree of deprotonation of HISA and the number of the coordinated hydroxide ions to the Pu^{4+} center within the identified complexes. For this purpose, the stoichiometry of each species was systematically modified at a constant charge (either -1 or -2) and the resulting structures were optimized and characterized by means

Tab. 3: Incorporation of U^{5+}/U^{6+} into magnetite (r in pm)

EXAFS					
U-O	U-Fe ₁	U-Fe ₂	U-O	U-Fe ₁	U-Fe ₂
218	319	355			
Fe ²⁺ /U ⁵⁺ (oct)			Fe ³⁺ /U ⁵⁺ (oct)		
DFT					
215	317	362	215	318	360
DFT+U					
219	310	363	219	311	362
Fe ³⁺ /U ⁶⁺ (oct)			Fe ³⁺ /U ⁶⁺ (tet)		
DFT					
222	308	360	215	345	354

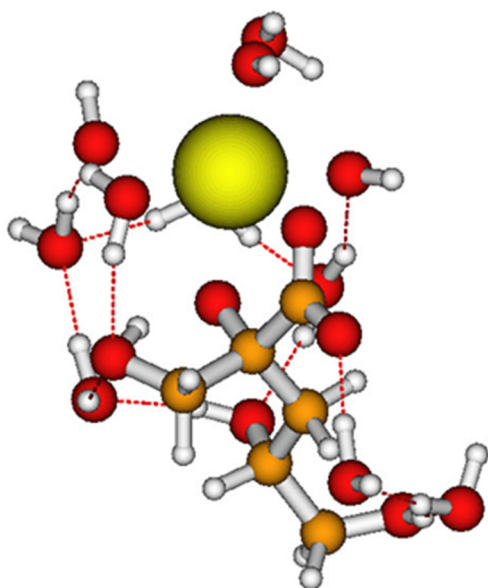


Fig. 3: Optimized $[Pu(OH)_3ISA-H]$ complex

of quantum chemical DFT calculations.

We used DFT(BP86/def2-SVP/epcIVmwb-avdz) calculations with f-in core pseudopotentials (epcIVmwb) and the corresponding GTO basis set at Pu^{4+} . This allows us to bypass any nondegeneracy of the ground state of the complex. The model system consisted of several water molecules and OH^- species around the metal ion and some additional water molecules at the acid. We found that a model system representing only the first water shell around the metal ion and the acid is sufficient for a realistic description of the system.

Complexes with the stoichiometries $Pu(OH)_3ISA_{-H}^-$ and $Pu(OH)_3ISA_{-2H}^{2-}$ were found to be the species with the lowest electronic energy for the charges -1 and -2 , respectively. For the $Pu(OH)_3ISA_{-H}^-$ species, the optimized structure (see Fig. 3) showed three OH^- ions bound to the Pu^{4+} cation, whilst the coordinating OH^- group of the ligand was deprotonated. Similarly, for the $Pu(OH)_3ISA_{-2H}^{2-}$ species the most stable structure indicates again the presence of three OH^- ions bound to the Pu^{4+} cation but with two OH^- groups of HISA deprotonated. The insights gained by DFT calculations are incorporated in the chemical and thermodynamic models derived from solubility data (see section 4.1).

Fundamental understanding of An(III)/Ln(III) separation with N-donor ligands

With the development of soft nitrogen based extracting ligands An(III) and Ln(III) can be separated efficiently reaching separation factors over 100. The origin of this separation as well as the failure of structurally similar ligands to accomplish separation is still a matter of controversy. Hence, we performed theoretical investigations of the ligands and their An(III)/Ln(III) complexes to shed further light on this origin.

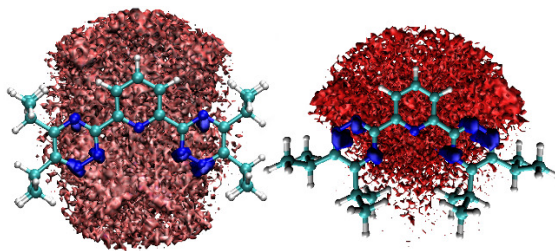


Fig. 4: 3D oxygen distribution function of the solvent molecules around iPr-BTP along the MD trajectory for cis/cis (left) and trans/trans (right) conformations within a 3.5 \AA radius of the pyridin nitrogen.

Before the formation of the metal-complex is modelled, a profound understanding of the ligand in solution is necessary in order to identify preorganization reactions and corresponding activation energies to transform the ligand into its conformation within the complex. These have been modelled by molecular dynamics (MD) simulations of the free iPr-BTP ligand in methanol/water mixtures of different molar fractions. Three different conformations of the triazine rings have to be taken into account, namely cis/cis, cis/trans and trans/trans. With increasing methanol concentration, the most favorable structures changes from cis/cis to trans/trans maximizing the accessible surface for lipophilic solvent molecules (see Fig. 4).

This is especially important for a deeper understanding of the processes during liquid-liquid extraction experiments. In upcoming simulations, the composition, width and shape of different liquid-liquid interfaces will be studied.

Considering metal-ligand complexes, a structural model is most important for further investigations. Especially the role of solvent molecules within the cluster formation is difficult to assess experimentally. Hence structure optimizations of possible Cm(III) complexes with two SO_3 -Ph-BTBP ligands and 0, 1 and 2 water molecules have been performed using density functional theory. All three structures proved to be true minima in gas-phase (Fig. 5).

Analysis of the reaction energies of the successive intrusion of water molecules into the first coordination shell shows the presence of one or two water molecules (Table 4). Herein, both thermodynamic contributions ΔE_{vib} as well as solvent contributions using the COSMO model have been included. For the latter, however, the explicit description of a full hydration shell would be necessary to shield the nega-

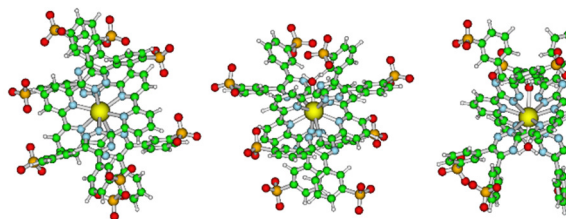


Fig. 5: Optimized complex structures of $[Cm(SO_3-Ph-BTBP)_2(H_2O)_n]^{5-}$ ($n=0,1,2$).

Tab. 4: Calculated energy differences for the reactions (1) intrusion of a first water molecule and (2) intrusion of a second water molecule.

	reaction (1) [kJ/mol]	reaction (2) [kJ/mol]
ΔE	-48.5	-7.4
ΔG	-57.4	-14.7
$\Delta E + \Delta E_{\text{vib}}$	-35.9	15.7

tively charged sulfonyl groups from the COSMO-surface. Hence the $\Delta E + \Delta E_{\text{vib}}$ reaction energies should be preferred.

Experimental confirmation was provided by means of TRIFS and vibronic side-band (VSB) spectroscopy in H₂O and D₂O. Fluorescence life-times decrease from 173 μs in H₂O to 374 μs in D₂O. Corresponding vibronic side bands have been found proving the theoretical prediction of water molecule presence in the first hydration shell. [3]

Fundamental understanding of An(III) versus Ln(III) bonding

Many attempts have been pursued to qualitatively and quantitatively describe covalency in metal-ligand bonding. The main problem herein lies within the rather vague definition of the term “covalency” itself. Theoretical studies, which are commonly based on electron density deformation and orbital analysis cannot be directly compared to experimental data, for example from NMR studies. Hence our aim is directed towards a systematic theoretical study of An(III) and Ln(III) bonding that allows an experimental verification of the computed trends. Throughout the last years a force field approach, describing charge/charge, charge/dipole and dipole/dipole interactions classically has been presented [4,5]. The dipole polarizabilities can be calculated accurately using multi-reference methods and relativistic basis sets. Obtained values for the dipole polarizabilities from NEVPT2 calculations for all non-closed-shell An(III) and Ln(III) ions are presented in Fig. 6. With the 5f electrons being less shielded by 6s and 6p electrons in the actinide ions compared to their lanthanide 4f counterparts, it is not surprising, that the An(III) polarizabilities are higher by a factor of almost 2 throughout the whole series.

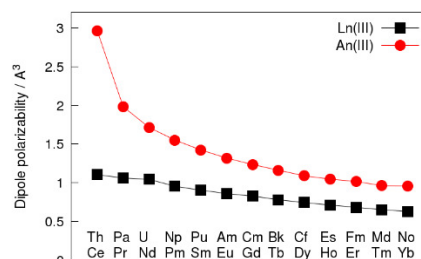


Fig. 6: Dipole-polarizabilities of Ln(III) and An(III) ions computed with the NEVPT2 method.

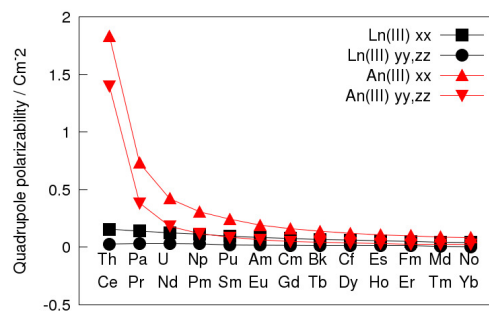


Fig. 7: Quadrupole-polarizabilities of Ln(III) and An(III) ions computed with the NEVPT2 method.

In order to clarify up to which order multipole moments are important in such an energy-decomposition scheme employed in force-field methods, it is necessary to consider quadrupole moments for these ions as well. Hence dipole-quadrupole- and quadrupole-polarizabilities have been computed for the same group of elements showing a similar trend with the actinide ions being more polarizable by a factor of up to 10 within the first half of the series (see Fig. 7). Future studies will quantify the implications of the An(III) versus the Ln(III) bond in detail.

References

- [1] Pidchenko *et al.*, Environ. Sci. Technol., 2017, 51 (4), pp 2217–2225
- [2] Glaus, M.A., et al., Environ. Sci. Technol., **42**, 2906-11, (2008).
- [3] Trumm *et al.*, Dalton Trans., 2016, 45, 12308
- [4] Trumm *et al.*, Mol Phys, 114, 876, 2016
- [5] Réal *et al.*, J. Phys. Chem. B, 114, 15913, 2010